

Tidal disruption near black holes and their mimickers

PRITAM BANERJEE,¹ SUVANKAR PAUL,¹ RAJIBUL SHAIKH,¹ AND TAPOBRATA SARKAR¹

¹*Department of Physics
Indian Institute of Technology
Kanpur 208016, India*

ABSTRACT

Black holes and wormholes are solutions of Einstein’s field equations, both of which, from afar, look like a central mass. We show here that although at large distances both behave like Newtonian objects, close to the event horizon or to the throat, black holes and wormholes have different tidal effects on stars, due to their respective geometries. We quantify this difference by a numerical procedure in the Schwarzschild black hole and the exponential wormhole backgrounds, and compare the peak fallback rates of tidal debris in these geometries. The tidal disruption rates in these backgrounds are also computed. It is shown that these quantities are a few times higher for wormholes, compared to the black hole cases.

1. INTRODUCTION

Tidal forces can tear apart a massive object due to the gravitational influence of another. This fact assumes importance in the context of supermassive black holes (BHs) with masses $M \sim 10^6 - 10^{10} M_\odot$ that are believed to exist at the center of most galaxies (see, e.g the reviews of Genzel et al. (2010), Kormendy and Ho (2013), Alexander (2017)). Stars that come in the vicinity of such large masses are often disrupted by extreme gravity (Lattimer and Schramm (1976), Evans and Kochanek (1989), Syer and Ulmer (1999), Magorrian and Tremaine (1999), Rosswog, Ramirez-Ruiz and Hix (2009), Shiokawa et al. (2015), see also the more recent review by Stone et al. (2019)), when the tidal forces become comparable to, or larger than, the self gravity of the star. Such tidal disruption events (TDEs) of stars in the background of a massive BH often produce an observable luminous flare, that can reveal important properties of the stellar structure (Lodato, King and Pringle (2009), Lodato and Rossi (2011), Metzger and Stone (2016), van Velzen et al. (2016)), as well as that of the BH (Kesden (2012), Zhang, Lu and Liu (2019)). Indeed, TDEs are known to be one of the main physical processes responsible for the formation of accretion disks around BHs (Cannizzo, Lee and Goodman (1990)), a topic that has received considerable attention of late, after the advent of the event horizon telescope (Akiyama et al. (2019)). Although several such TDEs have been observed, and seminal works have appeared in the literature over the last several decades, see, e.g Frank and Rees (1976), Lacy, Townes and Hollenbach (1982), Hills (1988), Rees (1988), Phinney (1989), it is perhaps fair to say that a complete theoretical understanding of these processes is still lacking. This assumes importance in the light of the Large Synoptic Survey Telescope (LSST)¹ which is expected to provide more data on TDEs in the near future.

In the context of a central mass M , the tidal radius $R_t \sim R_* (M/M_*)^{1/3}$, defined as the closest radial distance a stellar object of mass M_* and radius R_* can exist without getting tidally disrupted, is ubiquitous. This “1/3 law” is a standard textbook result where one uses the fact that at the tidal disruption limit, the tidal force equals the force due to self gravity at the surface of a star. This Newtonian result is true for any central mass M , regardless of the geometry that it produces, and it is perfectly legitimate to apply this to solutions of GR other than BHs, which might not have any obvious interpretation as a singularity covered by an event horizon. Indeed, while TDEs are believed to be common near galactic centers, relatively less attention has been paid in the literature to the fact that such objects that do not have an event horizon (i.e are not black holes) can also tidally disrupt stars. One such example is provided by the wormhole (WH) geometry. Wormholes are exotic solutions of GR that connect two different universes or two distant regions of the same universe via a throat, and continue to attract much attention,

Corresponding author: Tapobrata Sarkar
tapo@iitk.ac.in

¹ See <https://www.lsst.org/>

many decades after their inception. The original idea of the wormhole was related to a topology change of space-time by [Misner and Wheeler \(1957\)](#), and several notable attempts to understand the formation of such wormholes as a result of a phase transition were made in the early eighties by [Sato et al. \(1981\)](#), [Kodama et al. \(1981\)](#), [Maeda et al. \(1982\)](#). A traversable wormhole is one in which material particles can tunnel through the throat, and [Fuller and Wheeler \(1962\)](#) demonstrated that the Schwarzschild wormhole (or the Einstein-Rosen bridge) is not traversable. A detailed construction of a traversable wormhole appeared in the work of [Morris and Thorne \(1988\)](#) and soon after, the construction of a “time machine” based on this idea appeared in the works of [Morris, Thorne and Yurtsever \(1988\)](#), and [Novikov \(1989\)](#). For an excellent exposition to related details, see the book by [Visser \(1995\)](#) (see also the work of [Lemos, Lobo and Quinet de Oliveira \(2003\)](#) for related literature). It is well known that typically the matter required to support wormhole geometries will violate standard energy conditions in GR ([Morris and Thorne \(1988\)](#)). Various attempts have however been made to evade such violations and as is well known by now, dynamical solutions ([Kar and Sahdev \(1996\)](#)) or modified gravity ([Lobo and Oliveira \(2009\)](#)) might offer scenarios in which such a situation might be possible to envisage.

Quite naturally, wormholes continue to be a popular theme ever since these works, both at the technical level and in popular imagination, and as such are often treated at the same level as horizonless astrophysical objects. Indeed, a large amount of recent literature concerns astrophysical signatures of wormholes. For example, gravitational microlensing from wormholes were considered by [Abe \(2010\)](#), [Toki et al. \(2011\)](#), while [Takahashi and Asada \(2013\)](#) considered the cosmological constraints on these. Strong gravitational lensing by wormholes were recently studied by [Shaikh et al. \(2019a\)](#) and [Shaikh et al. \(2019b\)](#). Accretion disk properties of wormholes have been studied in [Harko, Kovacs and Lobo \(2008\)](#), [Harko, Kovacs and Lobo \(2009\)](#), and the more recent review of [Harko, Kovacs and Lobo \(2017\)](#).

Part of the reason that wormholes are exciting is that these can effectively mimic black holes. This was realized first by [Damour and Solodukhin \(2007\)](#). These authors pointed out that several detectable features of black holes, like quasi-normal modes and accretion properties as well as theoretical features like no-hair theorems can be very closely mimicked by wormhole solutions as well. In fact, after LIGO ([Abbott et al. \(2016\)](#)) announced the first evidences of gravitational wave detection, [Cardoso, Franzin and Pani \(2016\)](#) reported that a class of wormholes that have a thin shell of matter (with a specific equation of state) in the throat region can exhibit entirely similar quasi-normal mode ringing at early times compared to black holes, with differences being clear only at late times. Subsequently, [Konoplya and Zhidenko \(2016\)](#) showed that specific wormhole solutions can in fact exhibit quasi-normal mode properties that are similar to, or different from, black holes at all times. Clearly then, it is important and interesting to further the study of similarities between black holes and their wormhole mimickers, and in this work we study the differences in their TDEs.

As we have mentioned, our understanding of TDEs is far from complete. The main reason for this is the complicated nature of TDEs which rule out an exact theoretical treatment, and one has to resort to various approximations and costly numerical schemes. A part of the difficulty comes in due to the fact that one has to factor in effects of general relativity (GR) if stars come “close enough” to a BH ([Stone et al. \(2019\)](#)). To get an estimate of the numbers and the approximations involved, let us consider a typical $10^6 M_\odot$ BH at the galactic center. The Schwarzschild radius for such a BH is about a solar radius, R_\odot . By a conservative estimate, we can assume that GR effects will be small beyond $\sim 10R_\odot$, in which region one can safely resort to a Newtonian approximation. Then, the innermost stable circular orbit of the BH being at $6R_\odot$, such effects will be important if the TDE occurs in this BH background, between $6R_\odot$ and $10R_\odot$. For more general parabolic or highly elliptical orbits, the periastron position in Schwarzschild black hole (SBH) backgrounds can be as small as $4R_\odot$, providing even further room for the effects of GR to come into the picture. Such effects of GR on tidal disruption have been studied in several recent works in the context of BHs (see, e.g [Ishii and Shibata \(2004\)](#), [Ishii, Shibata and Mino \(2005\)](#), [Shibata and Taniguchi \(2008\)](#), [Kesden \(2012\)](#), [Zhou et al. \(2019\)](#)). The question that we ask here is related to such effects in WH geometries, which are relatively less studied. Indeed, far from a BH or a WH, there is no way to distinguish them from their TDEs, as these are effectively Newtonian, and hence the tidal radius will follow the power law discussed earlier. However, near the WH throat, something different is expected to happen. This is because near the throat of a WH, gravity is essentially repulsive in order to sustain the throat region, i.e to prevent it from collapsing. We therefore expect that close to the throat, WHs should behave very differently from BHs. It is in this region that GR becomes important, and hence one has to take care of GR effects carefully.

In this paper, we point out that GR might modify the tidal radius exponent, so that a more generic relation $R_t/R_* = \alpha(M/M_*)^\beta$, with $\beta \neq 1/3$ is a more appropriate working hypothesis in the region where GR effects are

important. The quantity R_* in this relation refers to the radius of the star in the absence of strong gravity. What we find from a numerical analysis is that the index β , as well as the proportionality constant α have different values for black hole and wormhole geometries. While for BHs, $\beta < 1/3$, for WHs on the other hand, $\beta > 1/3$. The index β plays a crucial role in the dynamics of the tidally disrupted matter. As is known, after a TDE, roughly half of the stellar mass remains bound, and starts coming back to the pericenter after a time $t_{min} \propto (\Delta\epsilon)^{-\frac{3}{2}}$, where $\Delta\epsilon$ is the dispersion in the energy of the tidal debris. Now, $\Delta\epsilon \sim R_t^{-2}$ (Phinney (1989)), so clearly any change in the index β from its Newtonian value will be important in determining the accretion rate. In this paper, we perform a numerical analysis adopting the method of Ishii, Shibata and Mino (2005) and determine the index β . This is then used to determine the peak accretion rate, and we show how differences with the Newtonian limit arise for stars that are tidally disrupted at distances close to the black hole event horizons or wormhole throats. Further, we study the rates of tidal disruptions in BH and WH backgrounds. These are also different due to reasons discussed above, and we quantify them in specific backgrounds.

This paper is organized as follows. In the next section, we will briefly review the relevant formalism and some of the main consequences of the deviation from the Newtonian power law. In section 3, we present our numerical analysis and determine this deviation, and revisit the consequences that it has on TDEs in black hole and wormhole backgrounds. Section 4 ends this paper with a summary of the main results.

2. METHODOLOGY

We will now discuss the methodology to be followed in this paper. These consist of three main ingredients, the space-time metric, the FN frame, and the numerical method to compute the tidal disruption radius.

2.1. Space-time metrics

The generic rotating vacuum solution to Einstein's field equations is the Kerr black hole (KBH), represented by the axially-symmetric metric written in Boyer-Lindquist coordinates,

$$ds^2 = - \left(1 - \frac{2GMr}{c^2\Sigma} \right) c^2 dt^2 - \frac{4GMra \sin^2 \theta}{c\Sigma} dt d\phi + \frac{\Sigma}{\Delta} dr^2 + \Sigma d\theta^2 + \left(r^2 + a^2 + \frac{2GMra^2 \sin^2 \theta}{c^2\Sigma} \right) \sin^2 \theta d\phi^2, \quad (1)$$

where $\Sigma = r^2 + a^2 \cos^2 \theta$ and $\Delta = r^2 + a^2 - 2GMr/c^2$. Here, M is the ADM mass, and with J being the angular momentum of the KBH, $a = \frac{J}{Mc}$ represents the spin parameter such that $0 \leq a \leq M$. The $a = 0$ limit of the Kerr metric yields the static, spherically symmetric Schwarzschild black hole (SBH) given by the metric

$$ds^2 = - \left(1 - \frac{2GM}{c^2 r} \right) c^2 dt^2 + \frac{1}{1 - \frac{2GM}{c^2 r}} dr^2 + r^2 d\theta^2 + r^2 \sin^2 \theta d\phi^2. \quad (2)$$

On the other hand, the quintessential example of a static traversable wormhole of the Morris-Thorne type is exemplified by the metric

$$ds^2 = -e^{2\Phi(r)} c^2 dt^2 + \frac{1}{1 - \frac{b(r)}{r}} dr^2 + r^2 (d\theta^2 + \sin^2 \theta d\phi^2). \quad (3)$$

The example that we consider here is the exponential wormhole (EWH) given by the functions

$$e^{2\Phi(r)} = e^{-\frac{2GM}{c^2 r}}, \quad b(r) = \frac{2GM}{c^2}, \quad (4)$$

where M is the ADM mass of the EWH.

A useful comparison of TDEs in black hole and wormhole backgrounds can be made by considering the SBH and the EWH, as the position of the throat in the latter geometry is at $r_{th} = \frac{2GM}{c^2}$, which is the same location as the Schwarzschild radius of the SBH. From a Newtonian perspective, an object that is captured by a SBH will tunnel through the throat of an EWH of the same mass.

2.2. The Fermi-Normal frame

We will consider parabolic (or highly elliptical) orbits in the backgrounds of the metrics mentioned above, in Fermi-Normal (FN) coordinates. The general formalism for space-times with spin is a convenient beginning point, from which static results can be obtained in the limit that the spin parameter goes to zero. For stationary backgrounds, we

will restrict only to the equatorial plane, where due to the axial symmetry, all the metric components are functions of r only. A star moving in a parabolic orbit close to the horizon of a BH or the throat of a WH will be influenced by the tidal fields of the BH and WH, respectively. GR effects are most conveniently studied by introducing a locally flat frame, called the Fermi Normal frame (Manasse and Misner (1963), Marck and Carter (1983)), that can move with the star along the geodesic where the time-like basis vector lies along the 4-velocity. The three other space-like vectors would be directed perpendicular to the 4-velocity. This way it is possible to describe the inhomogeneous nature of gravity namely the tidal fields, in terms of the flat space-like coordinates. Exactly on the geodesic, the tidal force is zero. As one moves away perpendicular to the geodesic, the tidal fields increases.

We will here display the FN coordinates for equatorial parabolic orbits in general spherically symmetric, static backgrounds, for simplicity, so that we can directly use them for both SBH and EWH. The same can be constructed for such orbits in the Kerr geometry as well (Marck and Carter (1983)), and we will present numerical results on these later. On the equatorial plane, a general spherically symmetric, static metric can be written as

$$ds^2 = -A(r)dt^2 + B(r)dr^2 + C(r)d\phi^2 . \quad (5)$$

Equatorial parabolic orbits specify the energy E and angular momentum L of a test particle as

$$E = 1 , \quad L = \sqrt{\frac{C(1-A)}{A}} \quad (6)$$

Now the Fermi Normal tetrad frame for an equatorial time-like geodesic can be written as

$$\begin{aligned} \lambda_0^\mu &= \left\{ \frac{E}{A}, \frac{\mathcal{P}}{\sqrt{B}}, 0, \frac{L}{C} \right\} \\ \lambda_1^\mu &= \left\{ \frac{\sqrt{BC}\mathcal{P} \cos \Psi}{\sqrt{B}\sqrt{A(C+L^2)}} - \frac{EL \sin \Psi}{A\sqrt{C+L^2}}, \frac{E\sqrt{AC} \cos \Psi}{A\sqrt{B(L^2+C)}} - \frac{L\mathcal{P} \sin \Psi}{\sqrt{B(L^2+C)}}, 0, -\frac{L\sqrt{L^2+C} \sin \Psi}{LC} \right\} \\ \lambda_2^\mu &= \left\{ 0, 0, \frac{1}{\sqrt{C}}, 0 \right\} \\ \lambda_3^\mu &= \left\{ \frac{\sqrt{BC}\mathcal{P} \sin \Psi}{\sqrt{B}\sqrt{A(C+L^2)}} + \frac{EL \cos \Psi}{A\sqrt{C+L^2}}, \frac{E\sqrt{AC} \sin \Psi}{A\sqrt{B(L^2+C)}} + \frac{L\mathcal{P} \cos \Psi}{\sqrt{B(L^2+C)}}, 0, \frac{L\sqrt{L^2+C} \cos \Psi}{LC} \right\} \end{aligned} \quad (7)$$

where we have

$$\mathcal{P} = \sqrt{\frac{E^2}{A} - \frac{L^2}{C} - 1} , \quad \frac{d\Psi}{d\tau} = \frac{ELC'}{2\sqrt{ABC}(C+L^2)} \quad (8)$$

The angle Ψ is introduced in order to parallel transport λ_1^μ and λ_3^μ along the time-like geodesic.

2.3. Numerical Procedure

As shown by Ishii, Shibata and Mino (2005), the tidal potential in the FN frame can be expressed upto fourth order in FN coordinates $\{x^0(=\tau), x^1, x^2, x^3\}$ as,

$$\phi_{\text{tidal}} = \frac{1}{2}C_{ij}x^i x^j + \frac{1}{6}C_{ijk}x^i x^j x^k + \frac{1}{24} [C_{ijkl} + 4C_{(ij}C_{kl)} - 4B_{(kl|n|}B_{ij)n}] x^i x^j x^k x^l + O(x^5) , \quad (9)$$

where the tensorial coefficients are defined as

$$C_{ij} = R_{0i0j}, \quad C_{ijk} = R_{0(i|0|j;k)}, \quad C_{ijkl} = R_{0(i|0|j;kl)}, \quad B_{ijk} = R_{k(ij)0} . \quad (10)$$

Here, the Latin indices i, j, k, \dots run over the spatial components 1 to 3. The symbols ‘;’ and ‘,’ indicate the covariant derivative and the ordinary (partial) derivative respectively. Moreover, $R_{0(i|m|j;k;l)}$ is a summation over all possible permutations of the indices i, j, k, l with m fixed at its position, and then division by the total number of such permutations. For orbits where the stellar radius is comparable to the periastron distance, the third and fourth order corrections become important. We consider a fluid star in the FN frame. Since the frame provides a locally flat surroundings around the star, it can be described by Newtonian gravity (Cheng and Evans (2013)). The hydrodynamic equation for this fluid star in presence of the tidal potential can then be expressed as

$$\rho \frac{\partial v_i}{\partial \tau} + \rho v^j \frac{\partial v_i}{\partial x^j} = -\frac{\partial P}{\partial x^i} - \rho \frac{\partial(\phi + \phi_{\text{tidal}})}{\partial x^i} + \rho \left[v^j \left(\frac{\partial A_j}{\partial x^i} - \frac{\partial A_i}{\partial x^j} \right) - \frac{\partial A_i}{\partial \tau} \right] \quad (11)$$

where the density, three-velocity ($\frac{dx^i}{d\tau}$) and pressure of the fluid are denoted by ρ , v^i and P , respectively. The last term on the right hand side of Eq. (11) arises due to the gravito-magnetic force (Thorne, Price and McDonald (1986)), and the corresponding vector potential reads, $A_i = \frac{2}{3}B_{ijk}x^i x^j$. Moreover, ϕ represents the Newtonian self-gravitational potential of the star, which obeys the usual Poisson equation,

$$\nabla^2 \phi = 4\pi G \rho . \quad (12)$$

The co-rotational velocity field of the fluid star in the FN frame can be assumed as

$$v^i = \Omega[-\{x^3 - x_c \sin \Psi\}, 0, \{x^1 - x_c \cos \Psi\}] , \quad (13)$$

where $\Omega = d\Psi/d\tau$. In presence of the third order terms of the tidal potential and/or the gravito-magnetic terms, the correction term x_c is non-zero, which corresponds to the fact that the rotational axis of the fluid star is different from the x^2 -axis and the position of its center of mass slightly deviates from the origin of FN frame. Its magnitude is very small compared to the radius of the star. Now, to simplify our calculation by eliminating Ψ , we consider another frame in which the star is kept fixed so that the frame itself rotates with respect to the original FN frame. Coordinates of the new tilde frame are related to the FN coordinates by

$$\tilde{x}^1 = x^1 \cos \Psi + x^3 \sin \Psi, \quad \tilde{x}^2 = x^2, \quad \tilde{x}^3 = -x^1 \sin \Psi + x^3 \cos \Psi . \quad (14)$$

Integrating the hydro-dynamic equation (Eq. (11)) using the expression of v^i (Eq. (13)), and then converting it to the tilde coordinates (\tilde{x}^i), we obtain

$$\frac{\Omega^2}{2} [(\tilde{x}^1 - x_g)^2 + (\tilde{x}^3)^2] = h + \phi + \phi_{\text{tidal}} + \phi_{\text{mag}} + C , \quad (15)$$

where C is an integration constant, $x_g = 2x_c$, and $h = \int \frac{dP}{\rho}$. Here, ϕ_{mag} is the gravito-magnetic scalar potential arising from the last term on the right hand side of eq.(11) involving A_i . Eqs. (12) and (15) are the two equations that we solve numerically to obtain our results. Let us now consider the polytropic equation of state of the star as, $P = \kappa \rho^{1+1/n}$. Here, κ is called the polytropic constant and n is the polytropic index. The entire numerical calculation is performed in units, $c = G = M = 1$. Moreover, we convert the basic equations (12) and (15) into dimensionless ones by using $\tilde{x}^i = pq^i$ to obtain numerical convergence, where the constant p has dimension of length and q^i 's are dimensionless. Therefore, in terms of q^i 's, the basic equations become

$$\nabla_q^2 \bar{\phi} = 4\pi \rho , \quad (16)$$

$$\frac{\Omega^2}{2} p^2 [(q^1 - q_g)^2 + (q^3)^2] = h(\rho) + p^2 (\bar{\phi} + \bar{\phi}_{\text{tidal}} + \bar{\phi}_{\text{mag}}) + C , \quad (17)$$

where $q_g = p^{-1}x_g$, $\bar{\phi} = p^{-2}\phi$, $\bar{\phi}_{\text{tidal}} = p^{-2}\phi_{\text{tidal}}$, $\bar{\phi}_{\text{mag}} = p^{-2}\phi_{\text{mag}}$, and ∇_q represents the Laplacian operator in q^i coordinates. Our purpose is to solve Eqs.(16) and (17) iteratively to find the critical value (ρ_{crit}) of the central density ρ_c for which the fluid star just remains in stable configuration in presence of the tidal field. A star having central density (ρ_c) less than ρ_{crit} will be tidally disrupted. To obtain the numerical solution, we consider a three dimensional cubical grid system of equal grid size in every direction with $101 \times 101 \times 101$ grid points. Complete detail of the step by step numerical procedure as well as determination of the constants, viz. C , p , q_g , etc from different boundary conditions can be found in Banerjee, Paul, Sheikh and Sarkar (2019). Once the critical central density (ρ_{crit}) and

Table 1. Numerical values of ξ_{R_*} and \mathcal{I} for different n

n	ξ_{R_*}	\mathcal{I}
1	π	39.478
3/2	3.654	34.106
3	6.897	25.362

the corresponding density profile of the star are obtained from the numerical analysis mentioned above, we find out

the critical mass of the star by integrating the density profile. Specifically, introducing the dimensionless parameters Θ and ξ , defined as, $\rho = \rho_c \Theta^n$ and $r = \bar{r} \xi$, where ρ_c is the central density and \bar{r} is a constant having dimension of length, the critical mass of the star comes out to be

$$M_\star = \frac{R_\star^3}{\xi_{R_\star}^3} \rho_c \left[4\pi \int_0^{\xi_{R_\star}} \Theta(\xi)^n \xi^2 d\xi \right] = \frac{R_\star^3}{\xi_{R_\star}^3} \rho_c \mathcal{I}, \quad (18)$$

where in the last relation one has to use the critical value ρ_{crit} of the central density ρ_c . We tabulate the values of ξ_{R_\star}

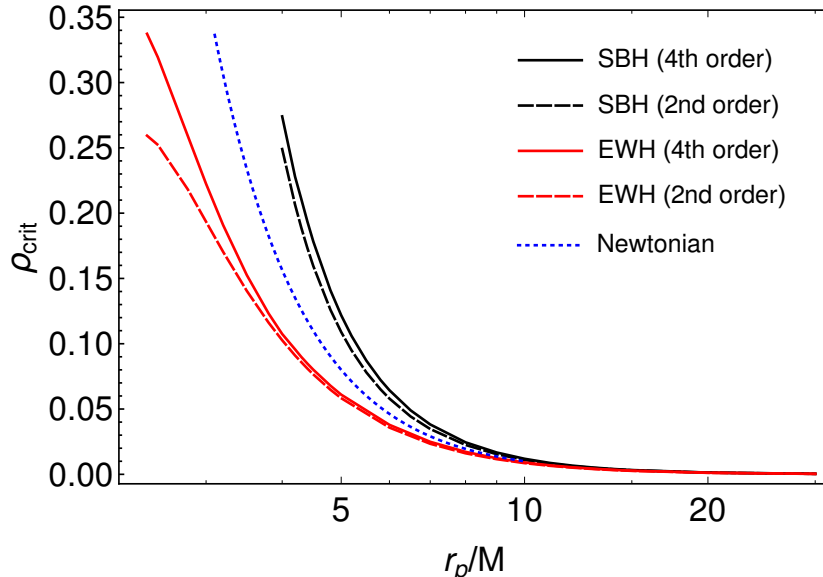


Figure 1. ρ_{crit} as a function of the periastron position r_p in logarithmic scale for the EWH and the SBH. Here, the masses of the EWH and the SBH have been set to 1 and so is the radius of the star. The Newtonian power law behaviour is also shown.

and \mathcal{I} in table (1), for different values of n . Here, ξ_{R_\star} corresponds to the value of the Lane-Emden parameter ξ at the surface of the star. Once we calculate the critical mass of the star, we fit this to a relation of the form

$$\left(\frac{R_t}{R_\star} \right) = \alpha \left(\frac{M}{M_\star} \right)^\beta. \quad (19)$$

We emphasize that all terms in Eq. (19) are in $c = G = M = 1$ units as described above. In Fig. (1), we show the variation of the critical central density (ρ_{crit}) as a function of the periastron position (r_p) for both the EWH and SBH, where we have taken the masses of the EWH and SBH to be unity, and have also considered, $R_\star = 1$. Table (2) shows the results of the fit mentioned in Eq. (19).

3. ANALYSIS

Here, we will present the implications of the discussion above. First, note that for a star to be tidally disrupted by a black hole (rather than being swallowed as a whole), we require the tidal radius to be greater than the radius of the event horizon. In contrast, for a wormhole, if the tidal radius is less than the radius of the wormhole throat, the object can tunnel through the throat into the universe on the other side. For the SBH, as already mentioned, the closest periastron position of the orbit is characterized by $r/M = 4$. From our numerical analysis, we find that for a star to be tidally disrupted at this value of the radius, one has, with $M = 1$, $\rho_c = 0.249$. The tidal disruption radius for the EWH of the same mass for the same value of ρ_c is $r/M = 2.531$. These values are conveniently tabulated in table (3), where we have also shown the value of the tidal radius for which a star is disrupted at $R_t/M = 4$ as given by a purely Newtonian analysis. The differences in the values of the various columns of R_t are then purely due to GR effects. The first two rows in table (3) corresponds to a second order GR calculation while in the last two rows we show the results up to fourth order in the tidal potential, which is important only for systems like a SBH-neutron

Table 2. Numerical values of $\alpha(n)$ and $\beta(n)$ for different n , for various backgrounds and fitting ranges

Object	Fitting Range	$\alpha(1)$	$\beta(1)$	$\alpha(1.5)$	$\beta(1.5)$	$\alpha(3)$	$\beta(3)$
SBH (2nd)	$4 \leq r/M \leq 12$	2.752	0.303	2.740	0.303	2.763	0.305
	$100 \leq r/M \leq 2000$	2.335	0.333	2.317	0.333	2.369	0.333
EWH (2nd)	$2.4 \leq r/M \leq 12$	1.842	0.374	1.832	0.375	1.835	0.380
	$100 \leq r/M \leq 2000$	2.318	0.333	2.317	0.333	2.369	0.333
SBH (4th)	$4 \leq r/M \leq 12$	2.866	0.298	2.852	0.299	2.862	0.302
	$100 \leq r/M \leq 2000$	2.338	0.333	2.320	0.333	2.372	0.333
EWH (4th)	$2.4 \leq r/M \leq 12$	1.918	0.370	1.904	0.371	1.917	0.374
	$100 \leq r/M \leq 2000$	2.323	0.333	2.320	0.333	2.372	0.333
KBH (4th) (a=0.9)	$1.8 \leq r/M \leq 12$	2.634	0.314	2.627	0.314	2.664	0.315
	$100 \leq r/M \leq 2000$	2.336	0.333	2.338	0.333	2.373	0.333
KBH (4th) (a=0.99)	$1.8 \leq r/M \leq 12$	2.591	0.317	2.584	0.318	2.621	0.319
	$100 \leq r/M \leq 2000$	2.336	0.333	2.338	0.333	2.373	0.333

Table 3. Numerical values of the tidal radius in units of $M = 1$ at second and fourth order

Order	ρ_c	R_t (N)	R_t (SBH)	R_t (EWH)
Second	0.249	3.430	4.00	2.531
	0.157	4.00	4.532	3.350
Fourth	0.274	3.320	4.00	2.740
	0.157	4.00	4.700	3.460

star binary. The value of ρ_c for which tidal disruption occurs at $r/M = 4$ for the SBH gives us the maximum possible difference between effects of TDEs in SBH and EWH backgrounds. From table (3), we see that for a $10^8 M_\odot$ SBH and an EWH of similar mass, the difference in the tidal disruption radius of a solar mass star is $\sim 10^{-5}$ light years. In table (4), we show the typical masses and radii of stars for which $\rho_c = 0.249$. For the last two rows in table (4), the fourth order results listed in table (2) are required.

Table 4. Numerical values of the masses and radii of stars with $\rho_c = 0.249$

M/M_\odot	M_*/M_\odot	R_* (cm)
10^8	1	4.69×10^{10}
10^6	0.7	1.93×10^9
10^5	0.7	4.16×10^8
10	1.4	1.09×10^6
5	1.4	6.89×10^5

Now, once the star is tidally disrupted, the spread of the specific energy of the debris is given from the expression of Stone, Sari and Loeb (2013) as $\Delta\epsilon = GMR_*/R_t^2$. Then, one obtains the minimum time required for the debris to come back to the pericenter (Lodato and Rossi (2011)) as

$$t_m = \frac{2\pi GM}{(2\Delta\epsilon)^{3/2}} \propto R_t^3. \quad (20)$$

The peak fallback rate, which is proportional to M_*/t_m can then be compared to the Eddington accretion rate, and for $R_* \sim R_\odot$ and $M \sim 10^6 M_\odot$, is typically a few orders of magnitude higher than the latter. Then, we see that the maximum value of the ratio

$$\frac{t_{m,EWH}}{t_{m,SBH}} = \frac{R_{t,EWH}^3}{R_{t,SBH}^3} = \left(\frac{2.53}{4}\right)^3 = 0.253. \quad (21)$$

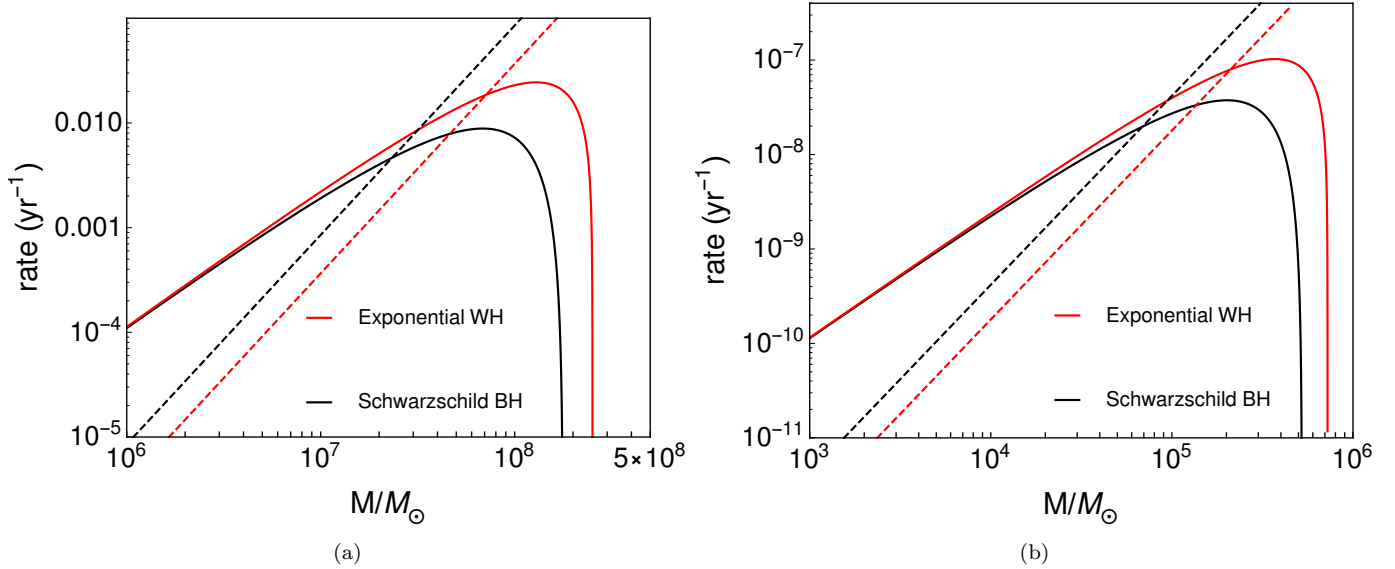


Figure 2. Variation of Γ_{TDE} with M (mass of the BH or WH) for a star having (a) mass M_{\odot} and radius R_{\odot} , and (b) mass $0.7M_{\odot}$ and radius 10^9 cm. The solid red curves represent EWH and the solid black curves correspond to SBH. The dashed lines denote the capture rate Γ_{cap} , with the same color coding.

Denoting the peak fallback rate as \dot{M}_p , the ratio of the rates, which is proportional to $1/t_m$ is then obtained as $\dot{M}_{p,EWH}/\dot{M}_{p,SBH} = 3.953$

Finally, we compute the tidal disruption rate of a star by Schwarzschild black hole or exponential wormhole. We assume a Maxwellian distribution of star velocities with a given number density n_d and velocity dispersion σ far from the BH or WH so that they follow highly elliptic or parabolic orbits to reach the minimum periastron position r_p near the BH or WH. In the process, stars are either tidally disrupted or directly captured by the BH or the WH depending on the r_p . If r_p is less than the tidal radius R_t it can be tidally disrupted. They are directly captured when the orbits enter the event horizon or the throat without tidal disruption. We assume that a star with a specific orbital energy E and angular momentum L approaches a BH or a WH. Following Kesden (2012), the capture rate is given by,

$$\Gamma_{\text{cap}} = \int_0^{L_{\text{cap}}} \frac{\partial \Gamma}{\partial L} dL = \frac{\sqrt{2\pi} n_d L_{\text{cap}}^2}{\sigma} \quad (22)$$

where, L_{cap} is the specific orbital angular momentum of the star below which it enters the event horizon or the throat without being tidally disrupted.

Similarly, tidal disruption rate Γ_{tidal} is obtained by evaluating the integration upto L_{tidal} , the specific orbital angular momentum below which the star enters the tidal radius R_t . Now, the tidal disruption event rate is obtained as, $\Gamma_{\text{TDE}} = \Gamma_{\text{tidal}} - \Gamma_{\text{cap}}$. In order to find L_{cap} or L_{tidal} we first choose the mass and radius of a star in units of $c = G = M = 1$, where M is the BH or WH mass. Then we put these values in eq.(18) to find out the critical central density for a given value of n . Once we have the critical central density, we can calculate the minimum possible r_p which the star can attain without getting tidally disrupted, i.e., $r_p = R_t$. Now, we put this r_p in eq.(6) to calculate L_{tidal} , whereas L_{cap} is the value of L for which $r_p = 4M$ for the SBH and $2M$ for the EWH.

Considering a constant density $n_d = 10^5 \text{pc}^{-3}$ and $\sigma = 10^5 \text{cm/s}$, the dependence of TDE rate with M is shown in figures (2(a)), (2(b)) and (3). Variation of the tidal disruption event rate Γ_{TDE} for solar mass stars, white dwarfs and neutron stars with BH or WH mass is shown. Here, the solar mass star with mass M_{\odot} and radius R_{\odot} , white dwarf with mass $0.7M_{\odot}$ and radius 10^9cm , and neutron star with mass $1.4M_{\odot}$ and radius 10^5cm are considered. The polytropic index is fixed at $n = 1$, along with $n_d = 10^5 \text{pc}^{-3}$ and $\sigma = 10^7 \text{cm/s}$. The solid red lines correspond to the EWH and the solid black lines for the SBH. The dashed lines denote capture rate Γ_{cap} , with the same color coding. For main sequence stars, the TDE rate vanishes for $M \sim 10^8 M_{\odot}$ or more. This suggests that main sequence stars are directly captured before getting tidally disrupted. White dwarfs are tidally disrupted if $M \sim 10^5$ or less, and neutron stars are only disrupted by stellar mass BH or WHs. The capture rate for the EWH is less than that of the SBH.

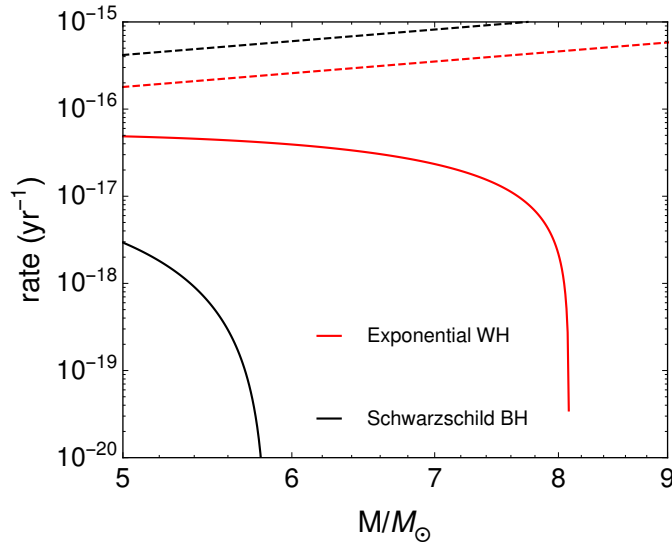


Figure 3. Variation of Γ_{TDE} with M (mass of the BH or WH) for a star having mass $1.4M_{\odot}$ and radius 10^7 cm. The color coding is the same as in Fig. (2).

This is due to the fact that the capture radius ($2M$) for exponential WH is smaller than the Schwarzschild BH. This suggests that the background geometry can make significant role in TDE rates.

4. SUMMARY AND DISCUSSION

Wormholes have various observational features that are similar to black holes and hence these can act as black hole mimickers. In this paper we have studied to what extent these behave differently as far as tidal disruptions are considered. This is important and interesting, as such tidal disruptions are one of the main reasons for the formation of accretion disks. From a Newtonian perspective, the ubiquitous “1/3 law” mentioned in the introduction determines the tidal radius for a given central mass, irrespective of its geometry. We have shown here that this rule is modified by strong gravity, in a way that can serve as a distinction between BHs and WHs. The physical reason for such a modification is that the physics near the black hole event horizon and that near the wormhole throat are very different. In the latter case, to sustain the throat so that it does not collapse, gravity might behave differently from that near a black hole horizon. Indeed, the deviation from the Newtonian result for the tidal radius is seen to be of opposite signs in the two backgrounds.

These effects might be important for observational distinctions, for example from data expected from the LSST. We have considered two such effects here. Firstly, we find that the peak fallback rate for wormholes might be about 4 times higher than that of a black hole with similar mass. Secondly, the tidal disruption rates for the wormhole examples we consider are greater than those for the corresponding black holes. Our analysis here is numerical, and specialized to a static scenario. A time-dependent analysis of tidal disruptions will be a natural extension of this work.

REFERENCES

- Abbott, B. P, *et al.* [LIGO Scientific and Virgo Collaborations], *Phys. Rev. Lett.* **116**, 061102 (2016).
- Abe, F (2010) *Ap. J* **725**, 787.
- Akiyama K, *et al.* (2019) *Ap. J* **875** no. 1, L1, no. 1, L2, no. 1, L3, no. 1, L4, no. 1, L5, no. 1, L6.
- Alexander, T, *Ann. Rev. Astron. Astrophys.* **55**, 1.
- Banerjee, P, Paul, S, Shaikh, R and Sarkar, T, *Phys. Lett. B* **795** (2019) 29-36.
- Cannizzo, J. K, Lee, H. M and Goodman, J (1990) *Ap. J* **351**, 38.
- Cardoso, V, Franzin, E, and Pani, P, *Phys. Rev. Lett.* **116**, 171101; Erratum: *Phys. Rev. Lett.* **117**, 089902.
- Cheng, R. M and Evans, C. R (2013) *Phys. Rev.* **D87**, 104010.
- Damour, T and Solodukhin, S. N, *Phys. Rev. D* **76**, 024016.
- Evans, C. R and Kochanek, C. S (1989) *Ap. J* **346**, L13.
- Frank, J and Rees, M. J (1976) *MNRAS* **176** 3, 633.
- Fuller, R. W and Wheeler, J. A (1962) *Phys. Rev.* **128**, 919.
- Genzel, R, Eisenhauer, F and Gillessen, S, *Rev. Mod. Phys.* **82**, 3121.

- Harko, T, Kovacs, Z and Lobo, F. S. N (2008) Phys. Rev. **D78**, 084005.
- Harko, T, Kovacs, Z and Lobo, F. S. N (2009) Phys. Rev. **D79**, 064001.
- Harko, T, Kovacs, Z and Lobo, F. S. N (2017) Fund. Theor. Phys. **189**, 63.
- Hills, J. G (1988) Nature **331**, 687.
- Ishii, M and Shibata, M (2004), Prog. Theor. Phys. **112** no. 3, 399.
- Ishii, M, Shibata, M and Mino, Y (2005), Phys. Rev. **D71**, 044017.
- Kar, S and Sahdev, D (1996) Phys. Rev. **D53** 722.
- Kesden, M (2012) Phys. Rev. **D85**, 024037.
- Kesden, M (2012) Phys. Rev. **D86** 064026.
- Kodama, H, Sasaki, M, Sato, K and Maeda, K (1981) Prog. Theor. Phys **66**, 2052.
- Konoplya, R. A, and Zhidenko, A, JCAP **12** 043.
- Kormendy, J, Ho, L. C (2013) Annu. Rev. Astron. Astrophys. **51**, 511.
- Lacy, J. H, Townes, C. H and Hollenbach (1982), D. J, Ap. J **262**, 120.
- Lattimer, J. M and Schramm, D. N (1976) Ap. J **210**, 549.
- Lemos, J. P. S, Lobo, F. S. N and Quinet de Oliveira, S (2003), Phys. Rev. **D68**, 064004.
- Lobo, F. S. N and Oliveira M. A (2009) Phys. Rev. **D80**, 104012.
- Lodato, G, King, A. R and Pringle, J. E (2009) MNRAS **392**, 332.
- Lodato, G and Rossi, E (2011) MNRAS **410** 359.
- Maeda, K, Sato, K, Sasaki, M and Kodama, H (1982) Phys. Lett. **B108**, 98.
- Magorrian, J and Tremaine, S (1999) MNRAS **309**, 447.
- Manasse, F. K and Misner, C. W (1963) J. Math. Phys. **4**, 735.
- Marck, J. A and Carter, B (1983) Proc. Royal. Soc. London **A385**, 431.
- Metzger, B. D and Stone, N. C (2016) MNRAS **461** no. 1, 948.
- Misner, C and Wheeler, J. A (1957) Ann. Phys. **2**, 525.
- Morris, M. S, and Thorne, K. S (1988) Am. J. Phys **56**, 395.
- Morris, M. S, Thorne, K. S and Yurtsever, U (1988) Phys. Rev. Lett. **61** 1446.
- Novikov, I. D (1989) JETP **95**, 769.
- Phinney, E. S (1989)in Morris M., ed., IAU Symp. **136**, Manifestations of a Massive Black Hole in the Galactic Center. Kluwer, Dordrecht, p. 543.
- Rees, M, J (1988) Nature **333**, 523.
- Rosswog, S, Ramirez-Ruiz, E and Hix, R (2009) Ap. J **695**, 404.
- Sato, K, Sasaki, M, Kodama, H and Maeda, K (1981) Prog. Theor. Phys. **65** 1443.
- Shaikh, R, Banerjee, P, Paul, S and Sarkar, T (2019) Phys. Lett **B789**, 270 (erratum: Phys. Lett. **B791**, 422).
- Shaikh, R, Banerjee, P, Paul, S and Sarkar, T (2019), JCAP **1907**, 028.
- Shibata, M and Tanighuch, K (2008), Phys. Rev. **D77**, 084015.
- Shiokawa, H, Krolik, J. H, Cheng, R. M, Piran, T and Noble, S. C (2015) Ap. J **804**, no. 2, 85.
- Stone, N, Sari, R, Lobe, A (2013) MNRAS **435**, 1809.
- Stone, N, Kesden, M, Cheng, R. M and van Velzen, S (2019) Gen. Rel. Grav. **51** no. 2, 30.
- Syer, D and Ulmer, A (1999) MNRAS **306**, 35.
- Takahashi, R and Asada, H (2013) Ap. J **768**, L16.
- Thorne, K. S, Price, R. H and MacDonald, D. A (1983) The Membrane Paradigm, Yale University, New Haven, CT.
- Toki, Y, Kitamura, T, Asada, H and Abe, F (2011) Ap. J **740**, 121.
- van Velzen, S et al. (2016) Science **351** no. 6268, 62.
- Visser, M (1995) Lorentzian Wormholes : From Einstein to Hawking, Woodbury, USA.
- Zhang, X, Lu, Y and Liu, Z (2019) Ap. J **877** no. 2, 143.
- Zhou, E, Tsokaros, A, Uryu, K, Xu, R and Shibata, M (2019) Phys. Rev. **D100** no. 4, 043015.